Available online at www.sciencedirect.com
SCIENCE DIRECT®
Physica D 190 (2004) 136–151
PHYSICA D
www.elsevier.com/locate/physd

External forcing of ecological and epidemiological systems: a resonance approach

Jon Greenman [a,*], Masashi Kamo [b,1], Mike Boots [c,2]

[a] *Department of Computing Science and Mathematics, University of Stirling, Stirling, FK9 4LA, Scotland, UK*
[b] *Department of Biology, Graduate School of Science, Kyushu University, Fukuoka 812-8581, Japan*
[c] *Department of Animal and Plant Sciences, University of Sheffield, Sheffield S10 2TN, UK*

Received 10 December 2002; received in revised form 12 August 2003; accepted 13 August 2003
Communicated by Y. Kuramoto

Abstract

Analysing ecological and epidemiological models is complicated by the multiplicity of states that can be excited in the interaction between model nonlinearity and external forcing. This multiplicity, typically created by a hierarchy of subcritical subharmonics, can lead to high amplification of the forcing signal and complex switching under chaos and stochastic externalities. Our objective is to understand the structure of these possible modes of system oscillation, in particular the conditions under which they appear and disappear. The analysis is carried out by transforming the problem into a problem of locating the resonances of the system under variable period forcing. The hierarchy of resonances identified has a well defined generic structure based on the natural period of oscillation of the model, whether stable or unstable when isolated. The usefulness and simplicity of this approach is illustrated in a discussion of a range of human diseases.

PACS: 89.60; 02.30.H

Keywords: Seasonal forcing; Resonances; Subharmonics; Epidemiology; Predator–prey

1. Introduction

The interplay between the internal nonlinear dynamics of ecological systems and various external factors that affect them, makes understanding population fluctuations a unique and challenging problem [1]. The most common manifestation of external forcing is through seasonality, including yearly variations in human activity (e.g. the school year cycle). Multiyear forcing can also occur, both naturally (e.g. the North Atlantic oscillation, the ice age cycle) and induced (e.g. forestry harvesting). The dynamical consequences of regular and stochastic external forcing are still poorly understood as are the underlying causes of the complex dynamical patterns that can occur in ecological models once forcing is applied.

Progress, however, has been made, particularly in the study of childhood diseases, using simple nonlinear models. Dietz [2], for example, studied the SIR model and Schwartz and Smith [3] the SEIR model to understand why diseases such as measles

* Corresponding author. Tel.: +44-1786-467460; fax: +44-1786-464551.
E-mail addresses: j.v.greenman@stir.ac.uk (J. Greenman), kamo@bio-math10.biology.kyushu-u.ac.jp (M. Kamo), m.boots@sheffield.ac.uk (M. Boots).
[1] Tel.: +81-92-642-2642; fax: +81-92-642-2645.
[2] Tel.: +44-114-2220054; fax: +44-114-2220002.

0167-2789/$ – see front matter © 2003 Elsevier B.V. All rights reserved.
doi:10.1016/j.physd.2003.08.008

and rubella were cyclical, typically peaking every 2 years in the case of measles and every 5 years for rubella in pre-vaccination data. These models do not have periodic solutions unless periodically forced, in which case they can then generate subharmonics, i.e. oscillations with period an integer multiple of the forcing period [4]. By simulation, Dietz [2] established the existence of a period 2 subharmonic for the SIR model with annual sinusoidal seasonality. The result was extended to the SEIR model by Aron and Schwartz [5]. They followed the subharmonic through a sequence of period-doubling bifurcations, a process leading to chaos [6]. In fact it was shown that subharmonics of all orders were possible and that more than one could exist simultaneously to create a multiple limit cycle system. An approximate algebraic integral condition for the existence of these subharmonics was obtained [3]. Step function seasonality has also been considered (to model more closely the school cycle) in the comparative study of childhood diseases by Keeling et al. [7], allowing the problem to be analysed as switching between attractors.

One important question raised by childhood and, indeed, other human diseases [8] is what determines which subharmonics dominate in given situations. The standard method of approach, to address this problem, is based on the bifurcation diagram in which one characteristic of a population variable (e.g. time-sliced value or maximum value) is plotted against one or more model parameters. Kamo and Sasaki [8], for example, took the bifurcation parameter to be the forcing amplitude (δ) and Earn et al. [9] the average contact rate (β_0) (as a proxy for birth rate) while Kuznetsov and Piccardi [10], in their two-dimensional study, varied both δ and β_0. Although such diagrams provide a geometric map of the bifurcations and show how they are connected (particularly [10]) there is little insight provided into why the diagram has the shape and structure that it has.

In this paper we present an alternative approach based on the familiar concepts of natural period and resonance rather than the complexities of bifurcation structure. This approach requires the model to be scaled to create a system with variable forcing period. The behaviour of the system is then defined by its hierarchy of nonlinear resonances [11]. This hierarchy has a transparent structure based on one key index, the natural period of oscillation of the system. The properties of the original (unscaled) model are obtained directly from the structural properties of the resonance hierarchy. This hierarchy is thought to be a feature of forced nonlinear differential equation systems in general, not just the S(E)IR model. The resonance approach is, therefore, likely to have wide applicability.

The paper is organised in the following way. In Section 2 we review the properties of the forced SIR model, using the bifurcation diagram approach to study its subharmonic states and the noise-induced switching between them. In Section 3.1 we explain the resonance approach, using the forced SIR model as a simple example to illustrate the methodology. In Section 3.2 we compare and contrast the bifurcation and resonance approaches and derive a set of simple rules to enable the resonance diagram to be sketched without the need for exhaustive simulation. In Section 3.3 we show the power of the resonance method by providing a simple explanation for why different diseases have different characteristics. In Section 4 we broaden the discussion by analysing models other than the S(E)IR model. We find that the same resonance structure is present in higher dimensional models, in models where externalities act through demographic terms, in models where the interaction terms take different functional forms and in ecological as well as epidemiological models. Even when the model is unstable when free, the resonance hierarchy can still be clearly identified when external forcing is applied.

2. The externally driven SIR model

2.1. The role of subharmonics

Consider the model [2] defined by the equations

$$\frac{\mathrm{d}S}{\mathrm{d}t} = \mu - \mu S - \beta IS, \tag{1a}$$

$$\frac{\mathrm{d}I}{\mathrm{d}t} = \beta IS - \gamma I - \mu I, \tag{1b}$$

$$\frac{dR}{dt} = -\mu R + \gamma I, \tag{1c}$$

where S, I and R denote susceptible, infectious and recovered populations, respectively. Since the natural birth and death rates are chosen equal (μ) and there is no infection-induced mortality, the total population: $H = S + I + R$ is constant and we normalise it to 1. Hence, only two of the three model equations are independent and need be considered in the analysis. Parameter γ is the rate of recovery from infection while β is the infection transmission constant (contact rate). When infection transmission is affected by external conditions β becomes a function of t. In the simplest case of seasonality we suppose that

$$\beta = \beta_0(1 + \delta\cos(2\pi t)) \tag{1d}$$

with β_0 and δ constant and 1 year as the unit of time. Parameters γ, μ, β_0 will be referred to, collectively, as the model parameters and δ as the (external) forcing parameter.

When there is no external forcing (i.e. $\delta = 0$) the system possesses a point equilibrium located at

$$S = \frac{1}{R_0}, \qquad I = \phi\left(1 - \frac{1}{R_0}\right),$$
$$R = (1-\phi)\left(1 - \frac{1}{R_0}\right), \tag{2}$$

where $\phi = \mu/(\gamma + \mu)$ and $R_0 = \beta_0/(\gamma + \mu)$, the basic reproductive rate [12]. This equilibrium is stable when relevant, i.e. when the infection rate exceeds the combined death and recovery rates at the start of the infection ($R_0 > 1$).

When the magnitude of the external forcing parameter δ is sufficiently small the system responds with oscillations of the same (annual) period as the external force. (We will refer to this as the base mode.) However with larger δ, simulation shows that stable subharmonics can be generated in which the system oscillates with a period that is an integer multiple of that of the external force [2]. This phenomenon is illustrated in the bifurcation diagram of Fig. 1a where the maximum of I (the infectious population) is plotted against the forcing parameter δ for each subharmonic in a hierarchy of subharmonics ranging from period 3 to period 9 in the interval $0 < \delta < 0.16$ [8]. These subharmonics emerge one by one through saddle-node (tangent) bifurcations in which a pair of limit cycles is created, one stable the other unstable. They are therefore subcritical [4] and appear without warning as the external force increases in magnitude. They do not necessarily appear in order of increasing period because

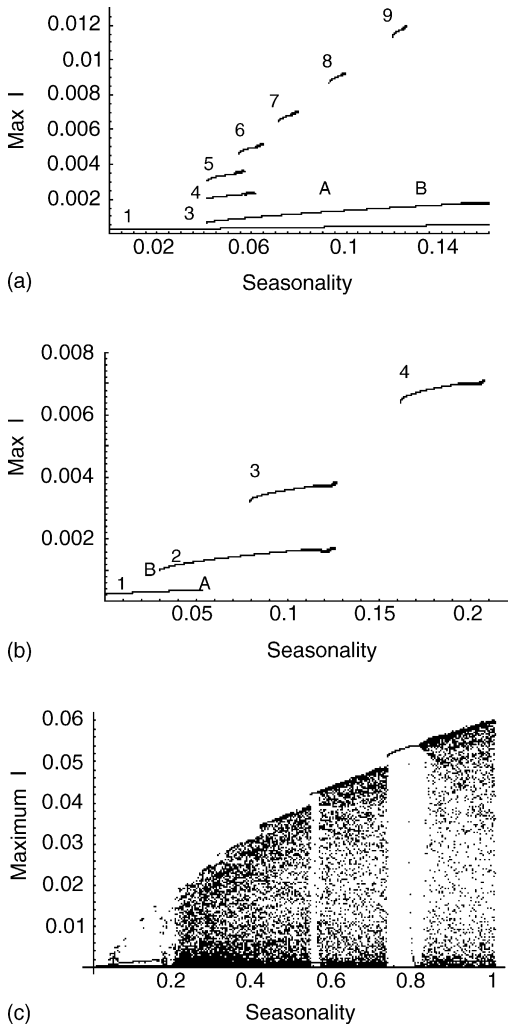

Fig. 1. The bifurcation diagram ($\max I$ vs. seasonality δ) for the SIR model ((1a)–(1d)) showing the hierarchy of subcritical subharmonics when (a) $(\gamma, \mu, \beta_0) = (40, 0.01, 500)$, $\delta < 0.16$; (b) $(\gamma, \mu, \beta_0) = (40, 0.01, 1300)$, $\delta < 0.22$. In (a) and (b) thicker line sections indicate period-doubling to chaos. Numbers denote the subharmonic period. In (b) there is subcritical period-doubling. Line AB indicates an unstable period 2 limit cycle. (c) Complete SIR bifurcation diagram for $0 < \delta < 1$. Parameters as in (a).

of the possible concavity of the saddle-node point envelope.

There are three special properties of these subharmonics that should be noted. Firstly, the amplitudes of the subharmonic oscillations are all greater than that of the base mode (period 1). For example, in Fig. 1a, the period 9 oscillation achieves a maximum population during its cycle 30 times greater than that of the base mode. Secondly, with the emergence of subharmonic modes, the system can have a choice of stable periodic states. It then becomes multistable. For example, for $\delta = 0.05$, there are four accessible stable modes of oscillation with periods 1, 3, 4 and 5 while for $\delta = 0.13$ there are three modes with periods 1, 3 and 9 (Fig. 1a). However, generally speaking, high period means small basin of attraction and hence a significant probability of switching to other modes of oscillation in the presence of noise [13]. Thirdly, with increase in δ the subharmonics apparently disappear as suddenly as they originally appeared. Simulation shows that this is brought about through period-doubling leading to chaos. Having reached chaos the system then seeks out an alternative but stable periodic state. For example when $\delta = 0.06$ the system switches from the now unstable period 4 to period 3 (Fig. 2a). The transient component of the time-series (Fig. 2a) suggests that the system is seeking the base mode but has to settle for the period 3 mode. In Fig. 2b, when $\delta = 0.17$, the system switches from period 3 to period 1, the base mode being the only stable periodic state available at this value of δ. In this second example the transient is chaotic (as confirmed by local Lyapunov exponent calculation), indicating the presence of a chaotic repellor [1,6,14,15].

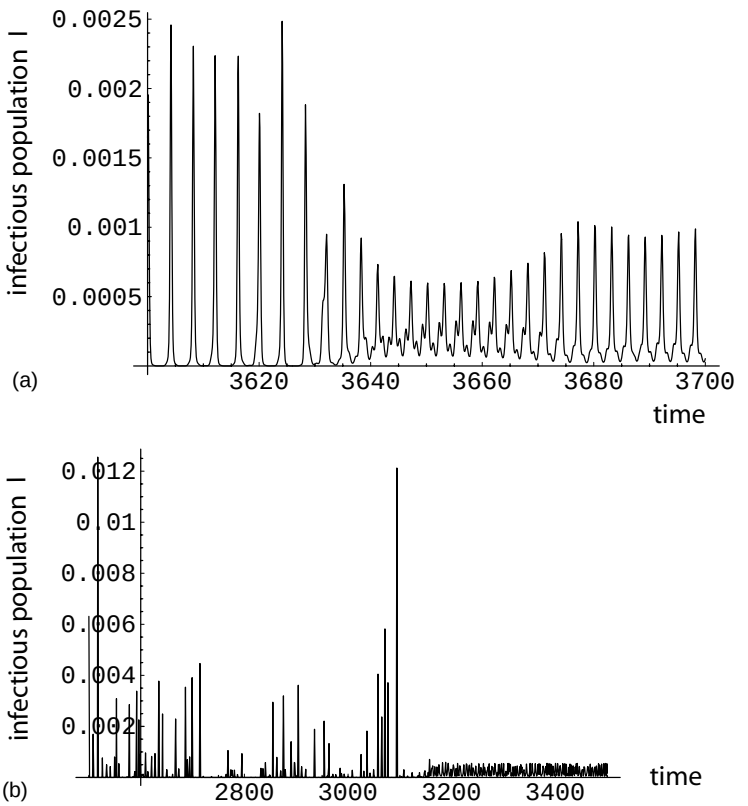

Fig. 2. Switching between SIR subharmonics. Instability leads to switching: (a) period 4 to period 3 ($\delta = 0.06$); (b) period 3 to period 1 with chaotic transient ($\delta = 0.17$). Model parameters as in Fig. 1a.

The subharmonic structure evident in Fig. 1a is robust to changes in the transmission constant β_0. However, if β_0 is decreased then less external forcing is required to excite a subharmonic but it has lower amplitude when excited. Conversely, if β_0 is increased then both δ and the amplitude are greater for a given subharmonic (Fig. 1b). One new feature with increase in β_0 is that the base mode (present for all values of δ in the relevance interval $0 < \delta < 1$ in Fig. 1a) bifurcates through period-doubling and the period 2 oscillation so created eventually becomes subcritical (Fig. 1b). This allows the possibility of hysteresis [4] to take place, with the system "jumping" between period 1 and 2 oscillations with slow variation in δ over an interval covering both points A and B in Fig. 1b. In addition to the oscillatory modes conforming to the hierarchical structure illustrated in Fig. 1a and b other subharmonics have been found seemingly bearing no relation to the hierarchy and stable only for short intervals in δ. Two such modes are shown in Fig. 1a,

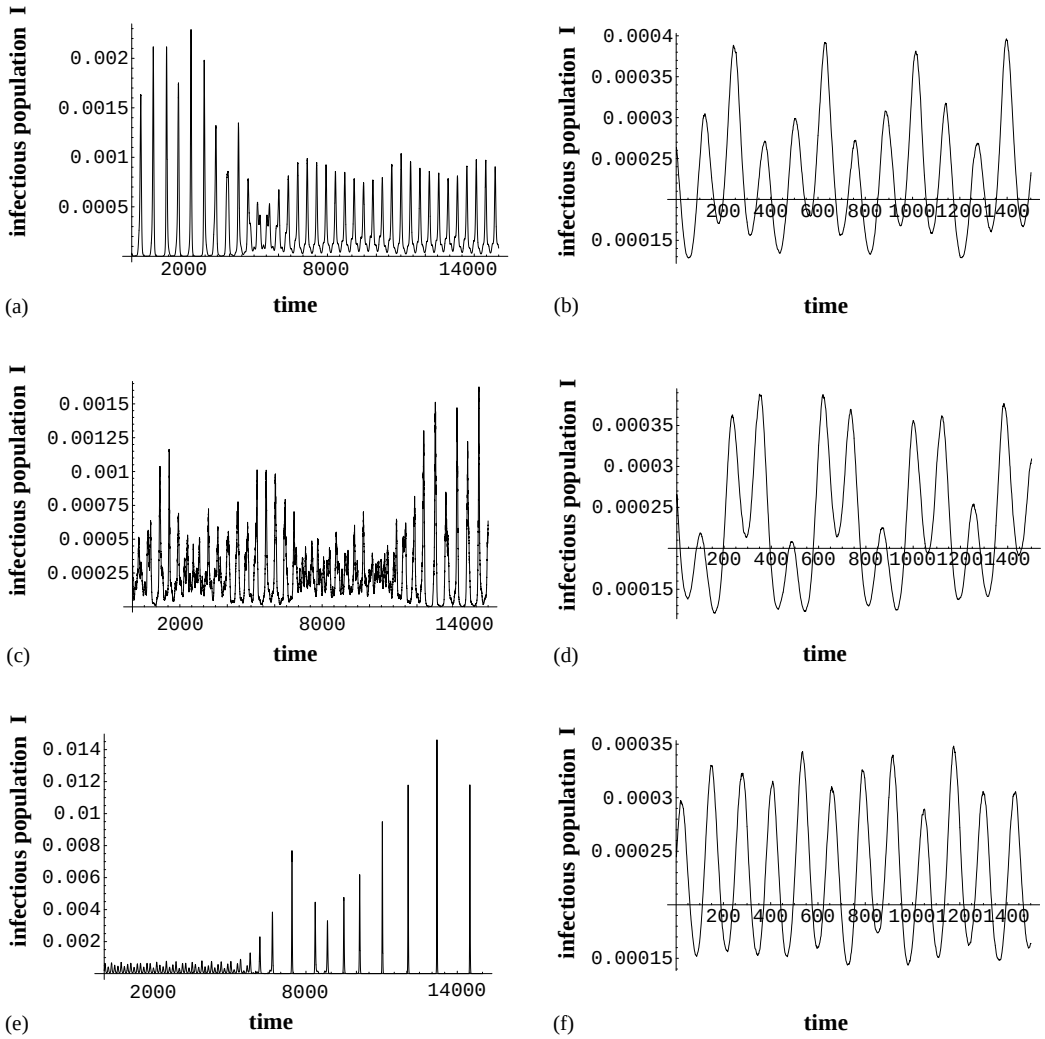

Fig. 3. The effect of noise on SIR subharmonic modes. (a) $\delta = 0.05$, S.D. $= 0.002$: switch from period 4 to period 3; (b), (d) and (f) $\delta = 0.05$, S.D. $= 0.003$: cycling between periods 3 and 1; (c) $\delta = 0.05$, S.D. $= 0.04$: bursts of differing periodicity (1, 3, 4); (e) $\delta = 0.17$, S.D. $= 0.005$; weak noise excites base mode back into chaos. (S.D.: noise standard deviation; other parameters as in Fig. 1a).

with period 7 occurring around point A and period 9 around point B (Fig. 1a). Their significance will be discussed in a later section.

For large enough δ ($\delta > 0.2$ in Fig. 1c) the dominant behaviour is chaotic punctuated with windows of periodicity. Each new chaotic interval is triggered by a subharmonic progressing through a period-doubling sequence, each such subharmonic forming part of the hierarchy previously identified [16,17]. For δ close to 1 in Fig. 1c the maximum infectious population is roughly 150 times the maximum level achieved in base mode.

2.2. The effect of noise

We have seen that even small changes in regular external forcing can have a dramatic effect on the behaviour of the system, by exciting large amplitude subcritical subharmonics. Weak noise can also have a disproportionate effect, for example by sustaining otherwise decaying oscillations [18–20]. To determine what happens when both weak noise and regular forcing are present, the model was discretised and multiplicative white environmental noise added to each equation. One might have expected that, with high period subharmonics vulnerable to being "kicked" out of their narrow basins of attraction, the system would spend most time in base mode, which has an extensive basin of attraction, trapped there by the weakness of the noise. This, in fact, does not necessarily happen as can be seen from Fig. 3a (S.D. ~ 0.002; S.D. = standard deviation) where the period 4 oscillation switches to period 3 (rather than period 1) after the noise is activated and this remains the case for less weak noise (S.D. ~ 0.005). However there is an intermediate range of noise strength (e.g. S.D. ~ 0.003) where the system approaches base mode but it can only do this by cycling between a period 3 and period 1 configuration (Fig. 3b, d and f). This is the opposite of "stochastic resonance" [21] since, in this case, switching between bistable modes suppresses the amplitude.

In a recent paper [15] it has been shown that noise applied to periodically forced systems can induce persistent chaotic behaviour in parameter regions well below the normal chaotic region. A sufficient condition for this to happen is the presence of two unstable periodic attractors associated, through period-doubling or saddle-node bifurcation, with stable periodic attractors. Whether this is a new system mode or a more precise way of describing noise-induced switching between modes merits further study.

It is important to note that noise primarily affects the amplitude rather than the periodicity of the system fluctuations [22,23]. This is true even for much stronger noise (S.D. ~ 0.04) when the system experiences bursts of periodic activity, switching between periodic modes, occasionally exciting period 4 and period 6 subharmonics (Fig. 3c).

With forcing parameter δ increased to a level where it is only the base mode that is stable (e.g. $\delta \sim 0.17$) the effect of even weak noise is to excite the base mode back into the chaotic state (Fig. 3e). The base mode is then intermittent [24] and the chaotic repellor has effectively been turned into an attractor [1]. With stronger noise, chaos can be intermittent with unstable higher period subharmonics.

3. The resonance approach

So far we have been content to describe rather than explain the deterministic behaviour of the SIR model. A deeper understanding can be obtained by transforming the model into one with resonant behaviour. This is achieved by scaling model Eqs. (1b) and (1c) by a constant factor p^{-1}, absorbing this factor within the model parameters: $\gamma' = \gamma/p$, $\mu' = \mu/p$, $\beta_0' = \beta_0/p$ on the right-hand sides of the equations and by rescaling time: $t' = tp$ on the left-hand side (and then, for convenience, dropping the primes). The equations then become

$$\frac{\mathrm{d}I}{\mathrm{d}t} = \beta IS - (\gamma + \mu)I, \tag{3a}$$

$$\frac{\mathrm{d}R}{\mathrm{d}t} = -\mu R + \gamma I, \tag{3b}$$

$$\beta = \beta_0 \left(1 + \delta \cos\left(\frac{2\pi t}{p}\right)\right). \tag{3c}$$

In the following analysis the new model parameters are fixed as p is varied. This means that we are tracing

a path through the original parameter space. Each value of p refers to a different member of the family of models defined by Eqs. (1a)–(1d). Systematically combining together the behaviour of the models on this path leads to a remarkably simple explanation of model behaviour. We have a model in which there is an external force with period, p, now a parameter. Varying this parameter reveals the many resonances excited by the external forcing.

3.1. The resonance diagram

We investigate the properties of model ((3a)–(3c)) by constructing its resonance diagram [11], with the maximum infectious population, $\max I$, plotted against the external period p for different values of δ. In Fig. 4a such a curve is shown for low δ ($\delta = 0.025$) and for the parameter values of Fig. 1a. There are three resonance peaks formed from the interaction between

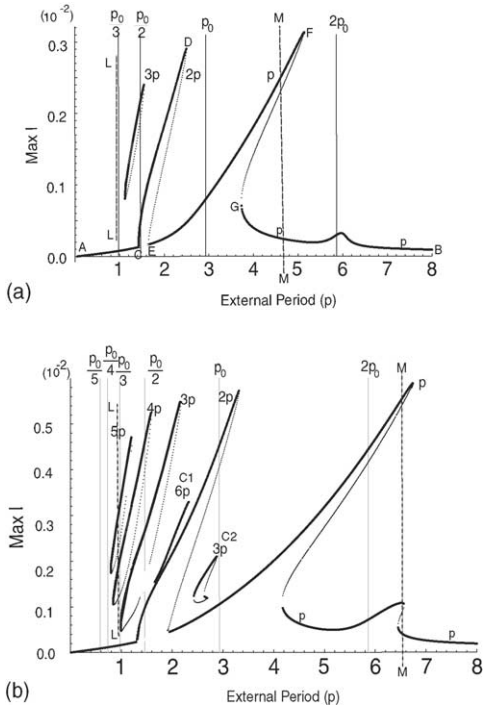

Fig. 4. SIR resonance diagrams for model ((3a)–(3c)) when (a) $\delta = 0.025$; (b) $\delta = 0.05$. Model parameter values as in Fig. 1a ($p_0 = 2.93$). Light dotted lines denote cyclic instability. The vertical lines: $p = (m/n)p_0$ intersect the p-axis at the resonance roots.

the external force and the natural mode of oscillation of the system. Although the isolated system is stable it typically reaches equilibrium through decaying oscillations. If their period is denoted by p_0 (the natural period of oscillation) there is resonance when $p \sim p_0$. Because of nonlinearity there is resonance also when $p \sim p_0/2$ and $p \sim 2p_0$. For the model shown in Fig. 4a, $p_0 \sim 3$ and hence the peaks are located at $p \sim 1.5$, 3 and 6. Nonlinearity not only produces multiple resonances but it also distorts the vertical shape of the familiar resonance curve found in linear theory, creating the "breaking wave" profile shown in Fig. 4a. This distortion also occurs in nonlinear mechanical and electrical systems as the analysis of the nonlinear pendulum shows [11,25,26]. The distortion bends the resonance peak to the right, to larger values of p, while the base of the resonance is anchored at the point on the horizontal axis through which the axis of the resonance would pass if the resonance were vertical and undistorted. We will refer to this point as the "root" of the resonance. For the nonlinear pendulum the property of leaning to the right is the result of dissipation [11], a likely explanation for the SIR model as well. The distortion of a resonance peak creates multiple states, as can be seen by taking vertical sections through the peak (e.g. MM in Fig. 4a). For each value of p lying in the "shadow" of the resonance there are three asymptotic states. The highest and lowest states are stable and the intermediate state unstable.

In interpreting the resonance diagram of Fig. 4a one should keep in mind the fact that there are three periods of interest: the natural system period p_0, the external forcing period p and the period of the system response, p_s. For the dominant peak, where the forcing period matches the natural period ($p \sim p_0$) the system responds to the external forcing with oscillations of the same period ($p_s = p$). However, for the peak at $p \sim p_0/2$ a subharmonic with period $2p$ is generated. The question naturally arises as to how these different system responses fit together on the continuous part, AB, of the resonance curve as p is varied (Fig. 4a). Detailed examination shows that at the start of the first resonance (at point C) there is period-doubling, generating the period $2p$ peak. At the peak itself (D) there is a saddle-node bifurcation connecting the stable

and unstable pair of period $2p$ limit cycles. At point E there is a pitchfork bifurcation [4] in which unstable period p and period $2p$ cycles combine to generate a stable period p oscillation. At the second peak (F) and at the lower point G there are saddle-node bifurcations.

Also to be noted in Fig. 4a is an apparently isolated section of the resonance diagram where the system executes oscillations of period $3p$. The significance of this component can be understood more clearly from the resonance diagram of Fig. 4b for the same model parameters as in Fig. 4a but for higher external forcing ($\delta = 0.05$). There is now a proliferation of the isolated components, including not only period $3p$ but also periods $4p$ and $5p$. They are in fact rooted to the family of points $p = p_0/n$ ($n = 3, 4, 5, \ldots$) on the p-axis and can be thought of as generalised resonances, "spray" rather than the "breaking waves" of the resonances grounded in base curve AB.

When δ is increased, the root of a resonance stays fixed (since p_0 does not depend on δ) but the resonance gains in height, while maintaining its slope, and broadens out, particularly at the base (compare Fig. 4a and b). In addition, more spray components are accessed, they are stretched in length in both directions and a succession of period-doubling bifurcations occur on each component, spreading from the centre. This creates a nested hierarchy of subharmonic sections with eventually an innermost section for which the system is chaotic. This mirrors the behaviour found in the corresponding bifurcation diagram. As δ is increased in Fig. 1a, each subharmonic follows the period-doubling route to chaos.

Conversely, if δ is decreased to zero then the subharmonic components disappear and the period 2 resonance rooted at $p_0/2$ shrinks in width and height until it also finally disappears, leaving the resonance at p_0 as the last remaining structural feature of the resonance diagram.

3.2. Interpretation

The connection between the two visualisations, the bifurcation diagram and the resonance diagram, can be made by taking the vertical section of the resonance diagram with the line $p = 1$ (LL in Fig. 4a and b). The intersections of this line with the resonances indicate which modes are likely to be active for the SIR model with the same model parameters as the resonance model ((3a)–(3c)) and the same δ defining the resonance diagram. For example in Fig. 4a there is intersection with only base mode (period 1) consistent with Fig. 1a where the vertical line: $\delta = 0.025$ also only intersects base mode. In Fig. 4b, however, there is intersection with subharmonics with periods 3, 4 and 5 as well, consistent with Fig. 1a with vertical line $\delta = 0.05$.

Which subharmonics can be accessed depends crucially on the value of p_0. In Fig. 4a and b it is about 3 in value but this can change significantly with change in model parameters. This natural period p_0 can be calculated from the formula

$$\varepsilon = R_0\phi, \qquad \theta = \sqrt{(\varepsilon - \phi) - \frac{\varepsilon^2}{4}},$$

$$p_0 = \frac{2\pi}{\theta(\gamma + \mu)}$$

(see (2) for definitions of R_0, ϕ). One conclusion we can draw from the resonance structure illustrated in Fig. 4a and b is that if $n - 1 < p_0 < n$ (n integer; $n > 2$) then the intersection line LL (Fig. 4b) is not likely to intersect subharmonic components with period less than np, since these components have their roots to the right of line LL and "lean" to the right. Therefore, the most likely subharmonic to be excited is the stable accessible subharmonic with the lowest period above the natural period ($p_s = np \sim p_0$). The external seasonal forcing term will tend, therefore, to sustain the otherwise decaying natural oscillations of the SIR model, a property in common with stochastic forcing [18]. This similarity in behaviour is evident in Figs. 2a and 3a.

It is also clear that the condition for there to be a subcritical period 2 subharmonic for the SIR model with $p = 1$ (as in Fig. 1b) is that $p_0 < 2$ for then the root of the period 2 resonance lies at $p_0/2$ to the left of the line LL. If δ is progressively reduced then the resonance shrinks until its base lies wholly to the left of LL, at some point ceasing to intersect LL, thereby creating a (subcritical) saddle-node bifurcation (Fig. 1b).

If p_0 is greater than but close to 2 in value then as δ is decreased the base of the period 2 resonance shrinks to lie entirely to the right of LL and in so doing the (supercritical) period-doubling bifurcation (from period 1 to period 2) is reversed.

The resonance diagram contains much more information about the original family of SIR models than is embodied in the intersection properties of line LL. In fact, if we take any vertical section (say, by the line $p = a$) then the behavioural modes intersected are active for the SIR model with parameters obtained by scaling up by factor "a" the parameters used in the resonance model ((3a)–(3c)) to construct the resonance diagram. For example, if we take $a = 0.95$ (in Fig. 4b) then the line $p = a$ does not intersect the resonant period 3 component and hence for the SIR model with parameters

$$\begin{aligned} v &= (\gamma, \mu, \beta_0) = (0.95)(40, 0.01, 500) \\ &= (38, 0.095, 475) = (0.95)v_0, \\ v_0 &= (40, 0.01, 500), \end{aligned}$$

this mode will not be excited by seasonal external forcing for the given value of δ. As a second example consider the intersection of the resonance curve with the line $p = 6.6$ in Fig. 4b. This line intersects two overlapping distorted resonance peaks ($p \sim p_0$, $p \sim 2p_0$) indicating the existence of five cyclic states with the same period ($p = 6.6$), all equal to the external forcing period. Three of these cycles turn out to be stable and two of them unstable. This means that the SIR model with parameters: $v = (6.6)v_0$ has three active stable cycles of period 1. As a third example, it is clear that only for those SIR models from the family corresponding to the resonance diagram of Fig. 4b that have parameters lying along the line section: $(1.3v_0, 3.1v_0)$ is the period 2 mode accessible (when $\delta = 0.05$).

In carrying out the calculations leading to the diagrams of Figs. 1 and 4 we have supposed that regular external forcing can be well described by a sinusoidal function (as in (1d)). To test the robustness of this choice of function we have repeated the calculations for both saw-tooth and step function periodicity. We have found that there is no substantial change in the results obtained provided the "standard deviations" of the forcing functions are comparable.

3.3. Applications

The bifurcation diagrams of Fig. 1a and b derive from the study by Kamo and Sasaki [8] of echoviruses as a causative agent of the aseptic meningitis epidemics in Japan. These diagrams show the sensitivity of the model output to the contact rate β_0. With β_0 high ($\beta_0 = 1300$; Fig. 1b) period 2 is the dominant subharmonic for weak forcing ($0.03 < \delta < 0.07$) while for much lower β_0 ($\beta_0 = 500$; Fig. 1a) the period 2 mode is not accessible and period 3 is the dominant subharmonic. In the resonance representation there is a simple reason for this. As we have seen, in the low β_0 case (Fig. 4a and b), the natural period is about 3 and so the resonance with root $p_0/2$ does not intersect the line LL ($p = 1$). This means that the period 2 mode is not excited. With high β_0 the natural period is lower at $p_0 = 1.7$ and hence $p_0/2 < 1$. There is now intersection with and excitation of the period 2 mode.

The resonance representation also helps to explain why in particular childhood diseases [7,27,28] only certain subharmonics appear. In Fig. 5 we have constructed resonance and also bifurcation diagrams for three such diseases: measles, whooping cough and rubella, based on the SIR model ((1a)–(1d)) using the pre-vaccination data of Keeling et al. [7] with $\delta \sim 0.2$. For measles the natural period is found to be 2.1 (Table 1), suggesting that for measles period 2 is just about accessible ($p_0/2 \sim 1$), given the spread in the resonance at its root, but the base mode is not accessible, having bifurcated to create period 2 (Fig. 5a). Also, the external forcing is sufficiently strong to excite periods 3, 4 and 5 and so strong that the intersection of LL with the $3p$ subharmonic occurs in

Table 1
The natural period for three childhood diseases (data from [7])[a]

	β_0	γ	p_0
Measles	476	28	2.1
Whooping cough	272	16	2.8
Rubella	140	20	4.1

[a] $\mu = 0.02$; unit: 1 year.

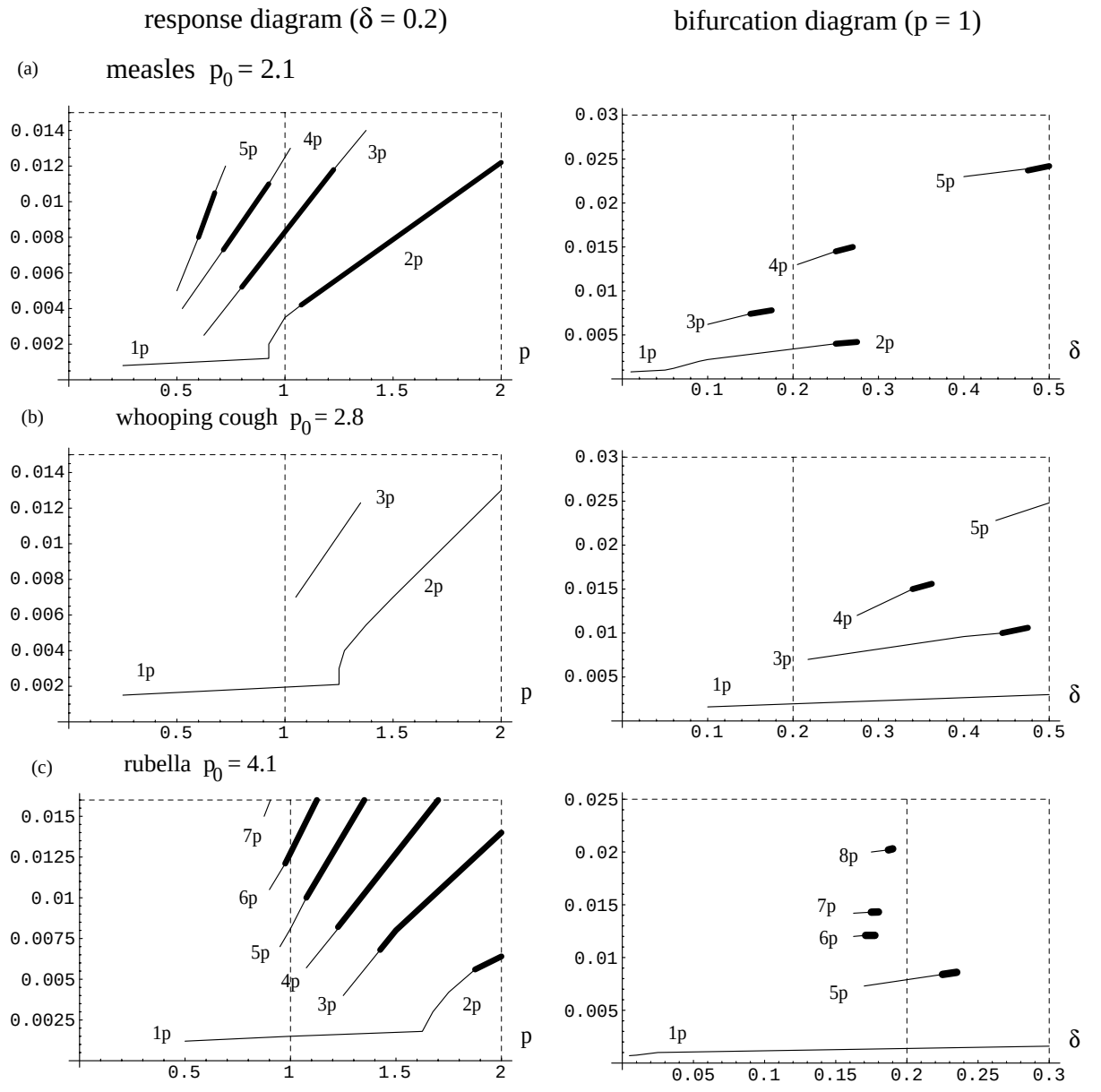

Fig. 5. The SIR resonance and bifurcation diagrams for: (a) measles; (b) whooping cough; (c) rubella. Parameters given in Table 1. For a resonance diagram thick line sections indicate where the system experiences period-doubling or transient chaos; for a bifurcation diagram these sections indicate period-doubling only.

transitional chaotic mode. Period 2 is the likely system outcome, close to the natural period of oscillation.

The natural period for whooping cough is 2.8 (with $p_0/2 > 1$), and hence period 2 is not accessible but base mode (period 1) is (Fig. 5b). Only the subharmonic with period 3 is excited at this level of forcing but it is not sufficient to stretch the $3p$ component enough to intersect line LL (Fig. 5b). An annual cycle is therefore expected for whooping cough. For rubella (with $p_0 = 4.1$), base mode is also accessible

but periods 2 and 3 are not since $p_0/n > 1$ for $n = 2, 3$ (Fig. 5c). Further, period 4 is not available when $\delta = 0.2$ (Fig. 5c) and so period 5 becomes the preferred subharmonic.

For stronger forcing ($\delta > 0.2$) different behaviour can occur. For rubella, for example, if $\delta = 0.55$ then the period 4 component is stretched sufficiently to intersect line LL (given the spread in this resonance at its root) and hence period 4 become active but it has lower amplitude because the intersection is closer to the axis. Similarly for whooping cough and period 3. For measles, for $\delta \sim 0.3$, behaviour would become chaotic with large amplitude fluctuations since there are no periodic modes of oscillation accessible, period 2 having become chaotic. With weaker forcing, it is also possible to excite new modes of oscillation. For example, for measles with $\delta \sim 0.125$ the period 3 cycle becomes non-chaotic to generate a bistable system with periods 2 and 3. Although period 2 is closer to the natural period, period 3 can be excited by external noise, at least during bursts of periodicity. Because, for measles, p_0 is close to but greater than 2 there will be a supercritical transition to base mode as δ is progressively reduced (Fig. 5a), not the subcritical transition evident in Fig. 1b.

The diagrams of Fig. 5 also provide an explanation for the different responses to noise. For measles and rubella, a variety of subharmonics can be excited, allowing a choice of (at least transient) periodic state when the system is disturbed by noise. For whooping cough, however, there is no periodic target subharmonic and, as a result, the system appears much more susceptible to noise.

4. External forcing of nonlinear systems

To support the argument that the hierarchical resonance structure is generic to forced nonlinear differential equation systems we have analysed a range of models, more complex than the simple forced SIR model ((1a)–(1d)). In particular we have looked at: (i) the SIR model with variable (density dependent) total population; (ii) the SIRV model [29,30] describing a vector-borne infection (with both constant and variable total population) (see Appendix A for details); (iii) a model for macroparasite infection transmitted through free-living stages [31]. The results show that the hierarchical structure is robust to these changes when external forcing acts through the host–infection interaction term. Forcing through the demographic terms also produced qualitatively similar resonance structure, although the system has to be forced much more strongly to produce the same level of structure. As an example we show in Fig. 6 the resonance diagram for the SIR model with external forcing applied through the natural birth rate (details can be found in Appendix A). Analysis of a predator–prey model with environmentally sensitive interaction term showed that the resonance approach is applicable also to trophic-web models with more general interaction terms [32].

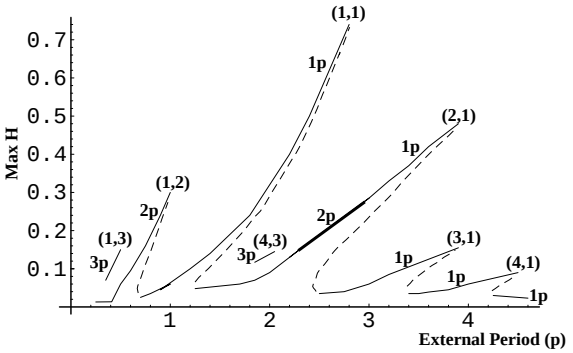

Fig. 6. Resonance diagram for the SIR model with density dependent regulation and demographic seasonality. Each resonance is indexed by the integer pair (m, n). Note the period-doubling on the (2, 1) resonance (for parameter values see Appendix A).

The SIRV and predator–prey models are both examples of a system which can become unstable even in the absence of external forcing. Since the discussion so far has been limited to the case where the resonance structure is based on excitation of otherwise decaying oscillations, the question arises as to what happens to this structure if the system is driven when in an unstable free mode. To answer this question we show in Fig. 7 the resonance diagram for the SIRV model for strong forcing and strong instability. (A similar diagram can be obtained for the predator–prey model.) The main resonance peaks still dominate the diagram

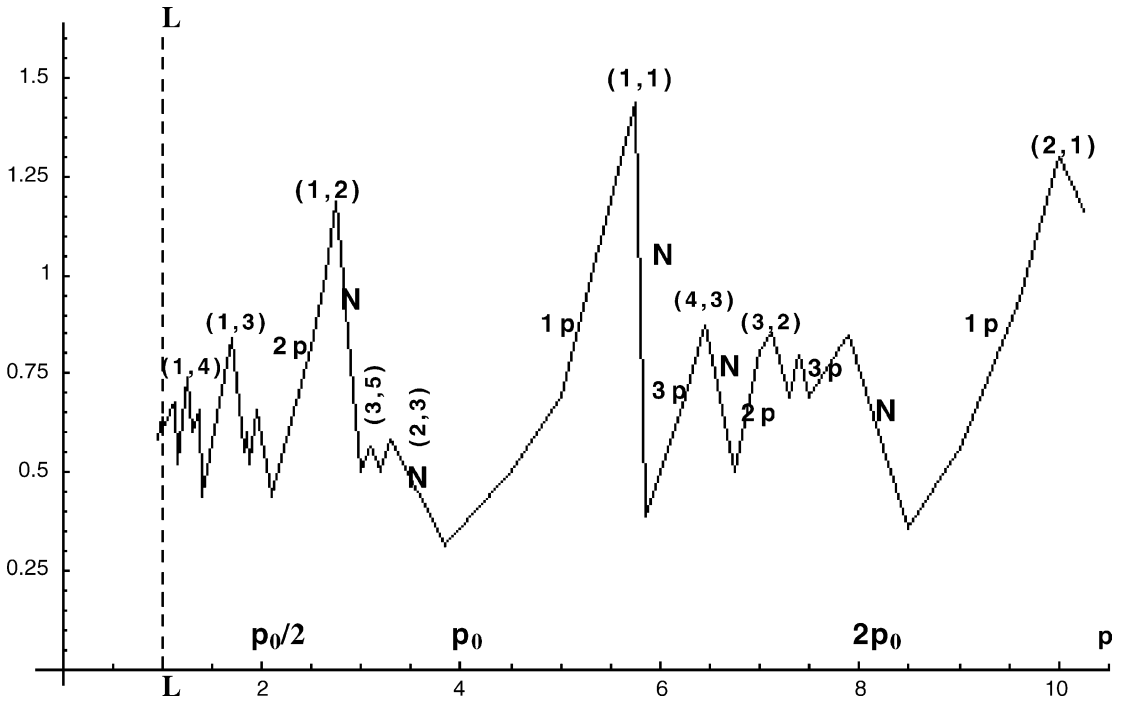

Fig. 7. Resonance diagram for the SIRV model with strong instability. Label N denotes non-periodic sections of the resonance curve. Integer pair: (m, n) indexes the resonances with np the system period (for parameter values see Appendix A).

but there are many other peaks appearing as well. Altogether, they form a double hierarchy of resonances indexed by two positive integers (m, n). The resonance (m, n) is rooted at $p = (m/n)p_0$ and on this resonance the system executes subharmonic motion with period $p_s = np(\sim mp_0)$. (The highest peaks correspond to $m = 1$.) Moving along a resonance (from left to right), the system is entrained as a subharmonic of the external forcing but beyond the peak the entrainment no longer holds and the amplitude collapses, in some cases to below that of the natural period of oscillations, manifesting destructive interference rather than enhancement through resonance. The double hierarchy can be traced back to the quasiperiodic oscillatory mode adopted by the system when the external and natural periods are incompatible. The system trajectories then lie on a torus and they never repeat their path unless the two periods are rationally related, i.e. there are two integers m, n (with, for convenience, no common factors), such that $p = (m/n)p_0$. Then the two periods are synchronised, the system response is periodic and entrainment is possible [11,33].

Quasiperiodicity first appears in the resonance diagram (for low values of p) as the SIRV model passes through its Hopf instability surface [4,30] but near that point the resonance diagram has a structure in all other respects similar to that shown in Fig. 4. As the strength of the instability increases (i.e. the distance from the instability surface increases) the second tier of resonances (with neither m nor n equal to 1) appear and merge with the existing resonances to form a continuum of successive subharmonic and non-periodic (i.e. quasiperiodic or chaotic) phases (Fig. 7). The sharpness in the collapse of the dominant resonance peaks reflects their "breaking-wave" origin.

Comparison of stable and unstable system resonance diagrams (Figs. 4b and 7) might suggest that only the dominant family $p/p_0 = m/n$ with m or $n = 1$ is present in the stable case but a closer look (Fig. 4b) suggests that there are other modes that can

be excited. Fig. 4b shows additional components C_1, C_2 and Fig. 1a "exotic" modes (points A, B) that fit in with the more general (m, n) hierarchy with neither m or n equal to 1. Precisely, at point A (Fig. 1a) $m = 2, n = 7$ (period 7), at point B $m = 3, n = 9$ (period 9) while for component C_1 (Fig. 4b) $m = 2, n = 6$ (period $6p$) and for C_2 $m = 2, n = 3$ (period $3p$). These values of m, n are determined from the system period (np) and from the position of the resonance root ($(m/n)p_0$).

Fig. 8b and c shows the time-series for two of these four "exotic" modes, together with their

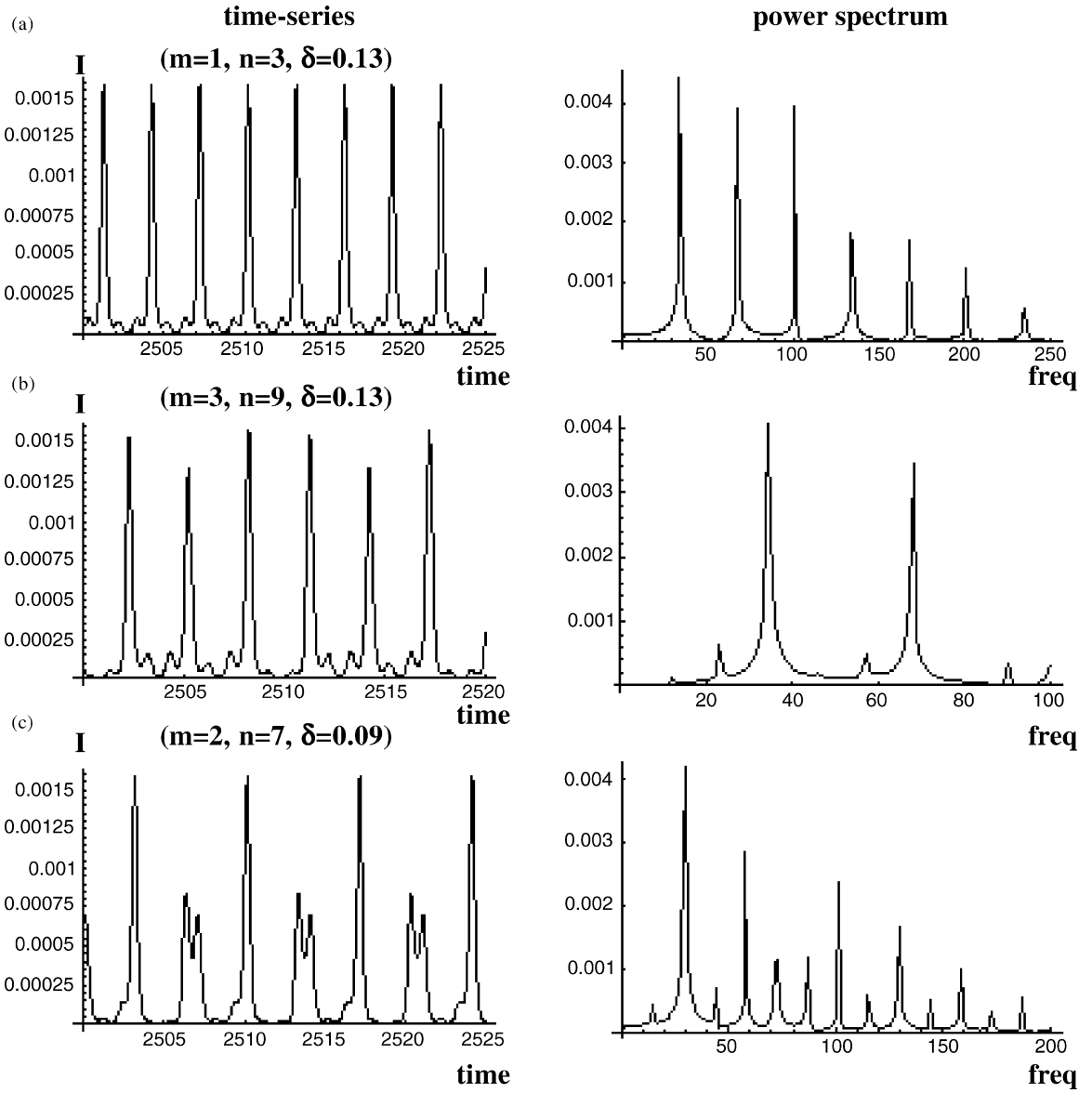

Fig. 8. The periodic time-series and power spectra for periodic modes shown in Fig. 1a: (a) period 3 for $\delta = 0.13$ ($m = 1, n = 3$); (b) "exotic" period 9 for $\delta = 0.13$ (point B) ($m = 3, n = 9$); (c) "exotic" period 7 for $\delta = 0.09$ (point A) ($m = 2, n = 7$). The (normalised) spectral frequency is calculated as $h/100$, where h is the horizontal coordinate.

power spectra. They are compared with a "normal" time-series, with $m = 1, n = 3$ (Fig. 8a). It is seen that the highest spectral peak occurs at frequency $100m/n$ and not $100/n$, emphasising the angular rather than the amplitude periodicity (i.e. the adjacent peak periodicity rather than the highest peak periodicity in the time-series).

5. Discussion

We have used two visualisation techniques to study the behaviour of a range of stable epidemiological models under external forcing: the bifurcation diagram and the resonance diagram. The bifurcation diagram shows the emergence, with increase in external forcing parameter δ, of a hierarchy of subcritical subharmonic modes of oscillation. That they have much larger amplitude than base mode means that substantial amplification of infection levels can take place if the system is encouraged to switch to a subharmonic mode. In transition, further amplification can occur if a subharmonic mode becomes unstable and the system moves into a chaotic state before finding an alternative stable periodic mode (e.g. Fig. 2b). We note that even weak noise can have a dramatic effect on the scale of the fluctuations. For example, it can turn a chaotic repellor into an attractor, restoring chaos to an otherwise stable base mode. Noise can also sustain the system above base mode and, when strengthened, can raise the system, at least for a time, into a higher subharmonic mode even though that mode may otherwise be unstable.

Although the bifurcation diagram is useful in identifying the different modes of behaviour of the system it does not provide much understanding of why these modes occur and how they fit together. The second representation, the resonance diagram, overcomes these problems. It is created by introducing a new (scaling) parameter, p, for the model parameters and for time, thereby making the period of external forcing variable. By plotting amplitude against period p a seascape of resonances is obtained rooted at the discrete points $p = (m/n)p_0$ where p_0 is the natural period and m, n are integers. Although the system may be some way from the familiar dominant resonance (with $m = n = 1$) it could very easily be in its shadow or near another member of the resonance family.

For models that are stable when isolated these resonances are of two types: isolated "spray" components representing higher subharmonics and the more familiar resonances of linear theory distorted by the nonlinearity, in some cases sufficiently to overlap and create multiple periodic states. For models that are unstable when isolated quasiperiodic modes of oscillation are present and a complex web of resonant modes are excited as instability and external forcing are increased.

Because the relationship between the original dynamic model and the resonance diagram is one of simple scaling one can relate back the properties of the resonance diagram to the properties of the original model by reversing the scaling. One important point to emerge from the analysis is that it is not only stochastic external forcing that sustains (otherwise decaying) natural system oscillations but regular forcing can also achieve this by its inability to excite lower subharmonics.

The power of the resonance approach is reflected in the fact that, once the natural period is known, the resonance diagram can be rapidly sketched without the necessity of extensive numerical calculation since the shape is generic. From the sketch one can predict what are the likely states to be excited and hence what the behaviour of the system will be under external forcing. The power has been shown in the analysis of models that describe human diseases. In a further paper we intend to apply the approach to other types of diseases, illustrating both stable and unstable model situations and comparing predictions with field data. In particular we will study the unstable model used by Dobson and Hudson [31] to test the hypothesis that the cycles observed in a red grouse population were caused by a macroparasite with free-living stages. Whether externalities can be as important a contributing factor is clearly a question of some interest.

The resonance approach can be extended to models, of whatever dimension, that can be suitably scaled. Indeed it was first introduced in this paper to analyse the two-dimensional SIR model ((1a)–(1d)) and

subsequently in the analysis of the four-dimensional self-regulated SIRV model (see Appendix A for details). We are currently applying the method to look at more structured epidemiological models, for example the SIR model with multiple pathogens or pathogen strains [8] and to externally driven multipatch models of disease transmission [34]. Equally amenable to analysis are trophic models with spatial heterogeneity [22,23,35] and subject to external forcing. In these cases there is the possibility of there being more than one natural period of oscillation, leading to an interweaving of resonance hierarchies.

What we have not attempted in this paper is an algebraic analysis of the resonance diagram, focusing instead on its qualitative properties. What would be useful is a formula for the resonance peaks that would specify the height and the distortion of these peaks in terms of the model parameters. Such formulae have been obtained, for example, in the analysis of nonlinear mechanical and electrical systems using both perturbation and averaging methods [11,25,36]. Typically these systems are much simpler to solve than the SIR type family of models since the external forcing is not applied through the nonlinear terms of the equation. We hope to report on progress with this problem in due course.

Acknowledgements

We would like to thank colleagues in the Institute of Biological Sciences and Rachel Norman and Jill Ireland in the Department of Computing Science and Mathematics at Stirling for helpful comments on the research presented in this paper. M.K. is supported by the Japan Society for the Promotion of Science. M.B. is a NERC Advanced Postdoctoral Fellow. The calculations were carried out with the software package Mathematica [37] on an AppleMac G4 computer.

Appendix A

Fig. 6 shows a resonance diagram for the variant of the SIR model in which density dependence (self-regulation) acts through natural mortality and seasonality through the natural birth rate. Precisely, the model is defined by the equations

$$\frac{\mathrm{d}H}{\mathrm{d}t} = (a-\mu)H - \alpha I, \tag{A.1a}$$

$$\frac{\mathrm{d}I}{\mathrm{d}t} = \beta_0 I(H-I-R) - (\mu+\alpha+\gamma)I, \tag{A.1b}$$

$$\frac{\mathrm{d}R}{\mathrm{d}t} = \gamma I - \mu R, \tag{A.1c}$$

$$\mu = \mu_0 + \mu_1 H, \qquad a = a_0(1+\delta\cos(2\pi t)), \tag{A.1d}$$

where H is the total population. Parameter "a" denotes the natural birth rate while parameters μ and α denote the natural and infection-induced mortality rates, respectively. In Fig. 6 the parameter values are taken to be

$$(a_0, \mu_0, \mu_1, \alpha, \gamma, \beta_0, \delta, p_0) = (1.83, 0.91, 0.0091, 43.34, 2.28, 85.41, 0.40, 0.92).$$

Fig. 7 shows a resonance diagram for the SIRV model [29,30] describing a vector-borne infection with seasonality acting through the infection transmission term. The model is defined by the equations

$$\frac{\mathrm{d}H}{\mathrm{d}t} = rH\left(\frac{1-H}{K}\right) - \alpha I, \tag{A.2a}$$

$$\frac{\mathrm{d}I}{\mathrm{d}t} = \theta\beta VS - (\gamma+\mu+\alpha)I, \tag{A.2b}$$

$$\frac{\mathrm{d}R}{\mathrm{d}t} = \gamma I - \mu R, \tag{A.2c}$$

$$\frac{\mathrm{d}V}{\mathrm{d}t} = \lambda I - (c+\beta H)V, \tag{A.2d}$$

$$\beta = \beta_0(1+\delta\cos(2\pi t)). \tag{A.2e}$$

Again H is the total host population (with K its carrying capacity) while V is the population of infective agents. Parameter r is the net natural birth rate at low densities, λ is the rate of host deposition of free-living stages, c the mortality of these stages and θ the average success of ingested infective agents in transmitting the infection. Parameters θ, K and δ are not scaled in the transformation leading to resonance. In Fig. 7 the parameter values are taken to be: $(\gamma, \mu, K, r, c, \alpha, A, \beta_0, \nu, \theta, \delta, p_0) = (0.0045, 0.011, 100.0, 1.0, 3.5, 7.5, 0.664, 2852, 1.0, 0.5, 4.05)$.

References

[1] O.N. Bjornstad, B.T. Grenfell, Noisy clockwork: time series analysis of population fluctuations in animals, Science 293 (2001) 638–643.

[2] K. Dietz, The incidence of infectious diseases under the influence of seasonal fluctuations, Lecture Notes in Biomathematics, vol. 11, Springer-Verlag, New York, 1976, pp. 1–15.

[3] I.B. Schwartz, H.L. Smith, Infinite subharmonic bifurcation in an SEIR epidemic model, J. Math. Biol. 18 (1983) 233–253.

[4] J. Seydel, Practical Bifurcation and Stability Analysis, Springer-Verlag, New York, 1994.

[5] J.L. Aron, I.B. Schwartz, Seasonality and period-doubling bifurcations in an epidemic model, J. Theor. Biol. 110 (1984) 665–679.

[6] W.M. Schaffer, Can nonlinear dynamics elucidate mechanisms in ecology and epidemiology? IMA J. Math. Appl. Med. Biol. 2 (1985) 221–252.

[7] M.J. Keeling, P. Rohani, B.T. Grenfell, Seasonally forced disease dynamics explored as switching between attractors, Physica D 148 (2001) 317–335.

[8] M. Kamo, A. Sasaki, The effect of cross-immunity and seasonal forcing in multi strain epidemic model, Physica D 163 (2002) 228–241.

[9] D.J.D. Earn, et al., A simple model for complex dynamical transitions in epidemics, Science 287 (2000) 667–670.

[10] Y.A. Kuznetsov, C. Piccardi, Bifurcation analysis of periodic SEIR and SIR epidemic models, J. Math. Biol. 32 (1994) 109–121.

[11] D.W. Jordan, P. Smith, Nonlinear Ordinary Differential Equations, Oxford University Press, Oxford, UK, 1999.

[12] R.M. Anderson, R.M. May, Infectious Diseases of Humans: Dynamics and Control, Oxford University Press, Oxford, UK, 1991.

[13] I.B. Schwartz, Multiple stable recurrent outbreaks and predictability in seasonally forced nonlinear epidemic models, J. Math. Biol. 21 (1985) 347–361.

[14] D.A. Rand, H.B. Wilson, Chaotic stochasticity: a ubiquitous source of unpredictability in epidemics, Proc. Roy. Soc. London B 246 (1991) 179–184.

[15] L. Billings, I.B. Schwartz, Exciting chaos with noise: unexpected dynamics in epidemic outbreaks, J. Math. Biol. 44 (2002) 31–48.

[16] C. Grebogi, E. Ott, Crises, sudden changes in chaotic attractors and transient chaos, Physica D 7 (1983) 181–200.

[17] H. Nagashima, Y. Baba, Introduction to Chaos, Institute of Physics, Bristol, UK, 1999.

[18] R.M. Nisbet, W.S.C. Gurney, A simple mechanism for population cycles, Nature 263 (1976) 319–320.

[19] V. Kaitala, E. Ranta, J. Lindstrom, Cyclic populations and random perturbations, Ecology 65 (1996) 249–251.

[20] J.V. Greenman, T.G. Benton, The amplification of environmental noise in population models: causes and consequences, Am. Nat. 161 (2003) 225–239.

[21] A. Bulsara, et al. (Eds.), Proceedings of the NATO workshop on stochastic resonance, special edition, J. Stat. Phys. 70 (1993).

[22] E. Mosekilde, Y. Maistrenko, D. Postnov, Chaotic Synchronization: Applications to Living Systems, World Scientific, Singapore, 2001.

[23] B. Blasius, A. Huppert, L. Stone, Complex dynamics and phase synchronization in spatially extended ecological systems, Nature 399 (1999) 354–359.

[24] Y. Pomeau, P. Manneville, Intermittent transition to turbulence in dissipative dynamical systems, Commun. Math. Phys. 74 (1980) 189–289.

[25] V.S. Anishchenko, et al., Nonlinear Dynamics of Chaotic and Stochastic Systems, Springer-Verlag, Berlin, 2002.

[26] J. Awrejcewicz, Bifurcation and Chaos in Simple Dynamical Systems, World Scientific, Singapore, 1989.

[27] B.F. Finkenstadt, B.T. Grenfell, Time series modelling of childhood diseases: a dynamical systems approach, J. Roy. Stat. Soc., Ser. C 49 (2000) 187–205.

[28] N.M. Ferguson, D.J. Noakes, R.M. Anderson, Dynamical complexity in age-structured models of the transmission of the measles virus: epidemiological implications at high levels of vaccine uptake, Math. BioSci. 138 (1996) 101–130.

[29] R.M. Anderson, R.M. May, The population dynamics of microparasites and their invertebrate hosts, Philos. Trans. Roy. Soc. London B 291 (1981) 451–524.

[30] D.M. Ross, Hopf bifurcations in ecological models: algebraic, geometric and numerical methods of analysis, Ph.D. Thesis, Department of Computing Science and Mathematics, University of Stirling, 2003.

[31] A.P. Dobson, P.J. Hudson, Regulation and stability of a free-living host-parasite system: *Trichostrongylus tenuis* in red grouse. II. Population models, J. Anim. Ecol. 61 (1992) 487–498.

[32] J.D. Murray, Mathematical Biology, Springer-Verlag, Berlin, 1993.

[33] R.M. Nisbet, W.S.C. Gurney, Modelling Fluctuating Populations, Wiley, New York, 1982.

[34] B.M. Bolker, B.T. Grenfell, Space, persistence and dynamics of measles epidemics, Proc. Roy. Soc. London B 348 (1995) 308–320.

[35] V.A.A. Jansen, The dynamics of two diffusively coupled predator–prey populations, Theor. Popul. Biol. 59 (2001) 119–131.

[36] J.K. Hale, Ordinary Differential Equations, Wiley–Interscience, New York, 1969.

[37] S. Wolfram, The Mathematica Book, Cambridge University Press, Cambridge, UK, 1999.